

Supporting Information

Nanoribbon Superstructures of Graphene Nanocages for Efficient Electrocatalytic Hydrogen Evolution

Ruchao Wei,^{a,#} Yu Gu,^{a,#} Lianli Zou,^{b,#} Baojuan Xi,^{*a} Yixuan Zhao,^a Yining Ma,^a Yitai Qian,^{a,c} Shenglin Xiong,^{*a} and Qiang Xu^{*b}

^a Key Laboratory of Colloid and Interface Chemistry, Ministry of Education, School of Chemistry and Chemical Engineering, and State Key Laboratory of Crystal Materials, Shandong University, Jinan, 250100, P. R. China

^b AIST-Kyoto University Chemical Energy Materials Open Innovation Laboratory (ChEM-OIL), National Institute of Advanced Industrial Science and Technology (AIST), Sakyo-ku, Kyoto 606-8501, Japan

^c Hefei National Laboratory for Physical Sciences at the Microscale and Department of Chemistry, University of Science and Technology of China, Hefei 230026, China

#These authors contributed equally to this work.

*Corresponding Authors.

E-mail: baojuanxi@sdu.edu.cn, chexsl@sdu.edu.cn, q.xu@aist.go.jp

Experimental section

Preparation of Ni-MOF-Rod

All chemicals were of analytical grade and directly used after purchase without any further purification. In a typical synthesis, nickel nitrate hexahydrate (1.7430 g, 5.994 mmol) was dissolved in 67.62 g dimethylformamide (DMF) with stirring to form a clear green solution (solution A). Then, 1,4-benzenedicarboxylic acid (H₂bdc, 0.9958 g, 5.994 mmol) was added to solution A and stirred until the solution become clear (solution B). Subsequently, 1,4-diazabicyclo[2.2.2]-octane (dabco, 0.3362 g, 2.997 mmol) was added to solution B and continually stirred for 2 h. The solution gradually turned into green suspensions, indicating that green solids had been formed in the system. The resulting mixture was transferred into a 100 mL Teflon-lined stainless-steel autoclave, placed in an oven and heated to 120 °C for 48 h. After cooling down to room temperature, the resulting green product was collected by centrifugation, washed thoroughly with DMF and absolute ethyl alcohol and finally dried at 70 °C.

Synthesis of SGNCs

Ni-MOF-Rods were dispersed in a ceramic boat and placed in a temperature-programmed tube furnace. After evacuation and Ar (99.999%) pumping three times, the temperature was raised from room temperature to a set temperature (400, 500, 600, 700, 800, 900 and 1000 °C) at a ramp rate of 2 °C min⁻¹ and kept at that temperature for 4 h under flowing argon gas. After that, the furnace was cooled down to ambient temperature naturally under an Ar flow. The resulting black materials (denoted as SGNC-*T*, *T* stands for the carbonization temperatures) were collected directly from the ceramic boat and used without further purification.

Characterization

The crystal structure of the products is characterized by power XRD (Bruker D8 Advance, Cu-K α radiation, $\lambda = 1.5406 \text{ \AA}$). The morphologies and microstructures are investigated by field-emission scanning electron microscopy (FE-SEM; GeminiSEM 300/500, 5kV) and field-emission transmission electron microscopy (TEM, HRTEM, and HAADF-STEM; JEOL ARM-200F, 200 kV; FEI Talos F200X TEM, 200 kV). The surface properties of the as-obtained samples are investigated by X-ray photoelectron spectroscopy (XPS, ESCALAB 250Xi, Thermo-VG Scientific, USA) with an Al K α X-ray source ($h\nu = 1486.6 \text{ eV}$) as the excitation source. Raman spectra are generated by Jobin Yvon LABRAM-HR confocal laser micro-Raman spectrometer. The porous texture properties of the samples are determined by measuring the nitrogen adsorption–desorption isotherms (an Autosorb 6B instrument) at 77 K. FTIR spectra were recorded on a Bruker ALPHAT FTIR spectrometer through the KBr disk method in the range 4000-400 cm^{-1} . Thermogravimetry analysis was conducted on a Mettler Toledo TGA/SDTA851 thermal analyzer in N₂ with a heating rate of 10 $^{\circ}\text{C min}^{-1}$ from room temperature to 800 $^{\circ}\text{C}$. CHN elemental analysis were conducted on a Elementar Vario EL Cube CHNS elemental analyzer.

Electrochemical measurements

The electrochemical measurements were carried out with a three-electrode cell using a potentiostat. To prepare the working electrode, 10 mg electrocatalyst and 50 μL Nafion (5 wt% in a mixture of lower aliphatic alcohol and water, Aldrich Chemical) were dispersed in 1 mL water/ethanol (v:v, 3:1) solution by sonication to form a dispersion.

The electrocatalyst suspension (10 μL) was loaded onto a rotating disk electrode (RDE) with a diameter of 5 mm (loading amount $\sim 0.485 \text{ mg cm}^{-2}$). Linear sweep voltammetry was conducted in N_2 saturated 1.0 M KOH and 0.5 M H_2SO_4 with a scan rate of 5 mV s^{-1} and a rotation speed of 1,600 r.p.m. The Ag/AgCl (saturated KCl) electrode and graphite rod were used as the reference electrode and counter electrode, respectively. The RDE loaded with various samples served as the working electrode. All potentials were referenced to the reversible hydrogen electrode (RHE). To measure the ECSA, we employed the double-layer capacitance formulation to compare the active surface area of our prepared electrocatalysts. The capacitance was measured using cyclic voltammetry with a scan rate in the range from 20 to 120 mV s^{-1} in a non-Faradaic potential window of 0.1 to 0.2 V versus RHE in 1 M KOH.

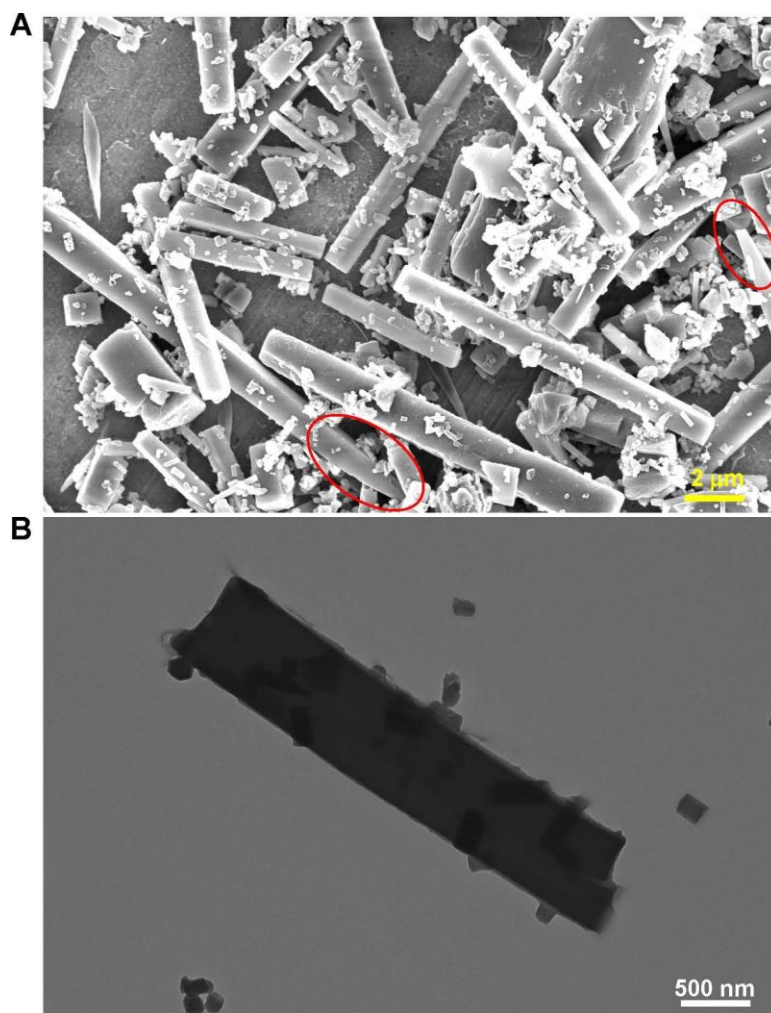


Figure S1. (A) FE-SEM and (B) TEM images of the rod-shaped Ni-based MOF.

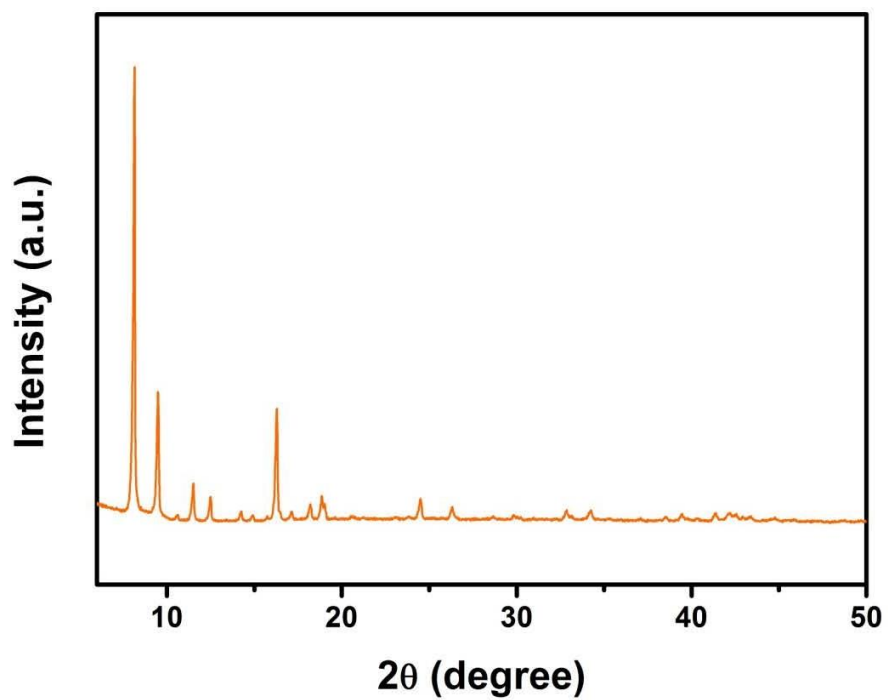


Figure S2. XRD patterns of the rod-shaped Ni-based MOF.

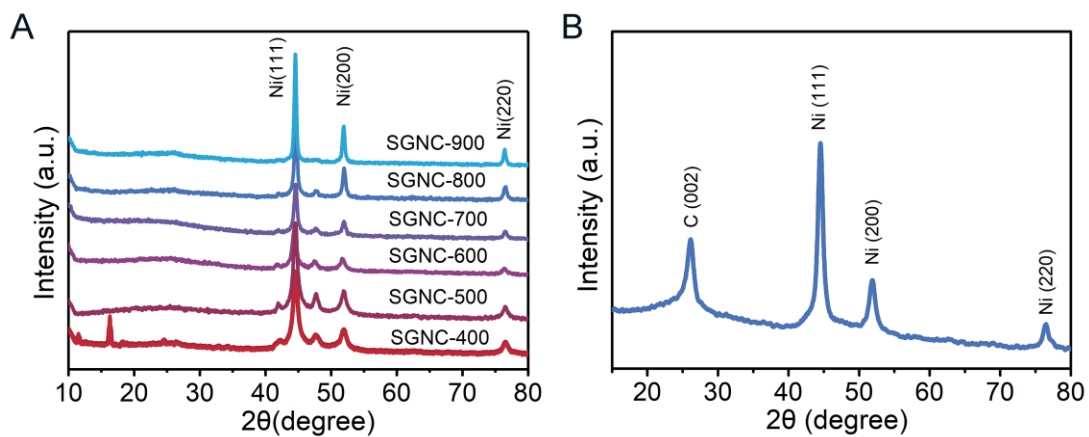


Figure S3. (A) XRD pattern of SGNCs obtained under different calcination temperatures. (B) XRD pattern of SGNC-900 (after the acid treatment).

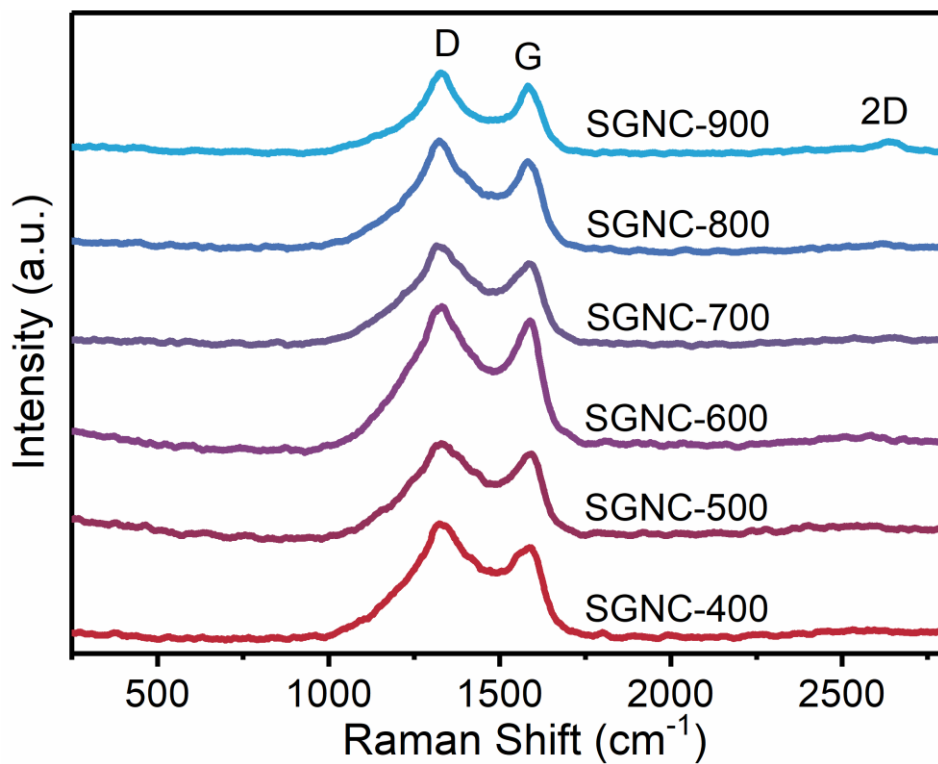


Figure S4. Raman spectra of SGNCs obtained under different calcination temperatures.

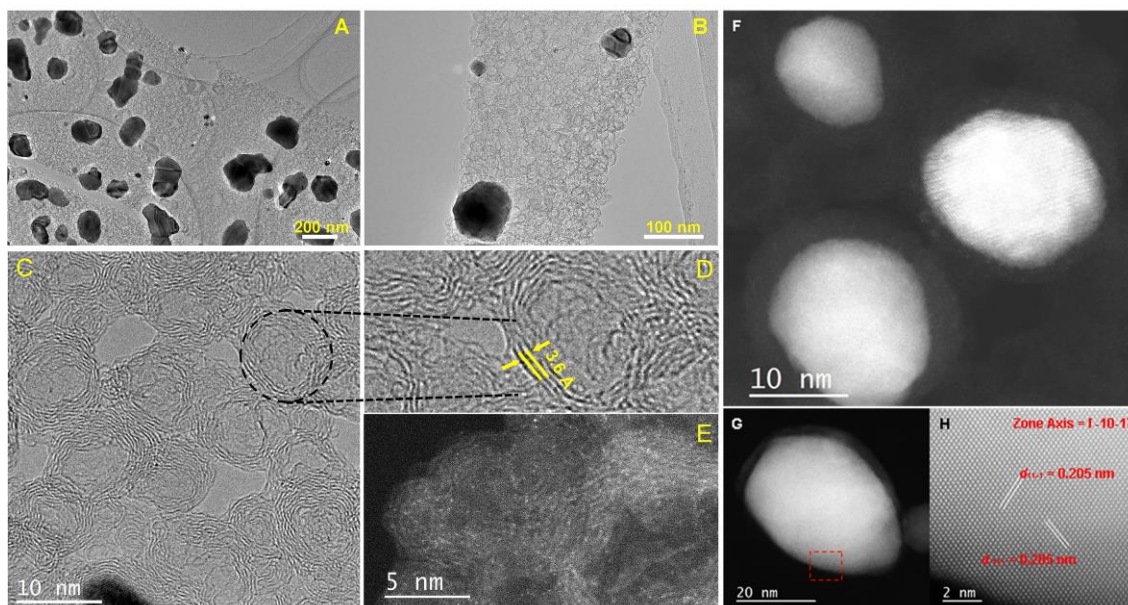


Figure S5. (A,B) TEM images of SGNC-900. (C,D) HRTEM images of SGNC-900. (E) HAADF-STEM image of graphitized carbon nanocages (GCN). (F) HAADF-STEM image of few-layer graphene coated Ni NPs. (H) HAADF-HRTEM images recorded from a marked with red boxes in (G).

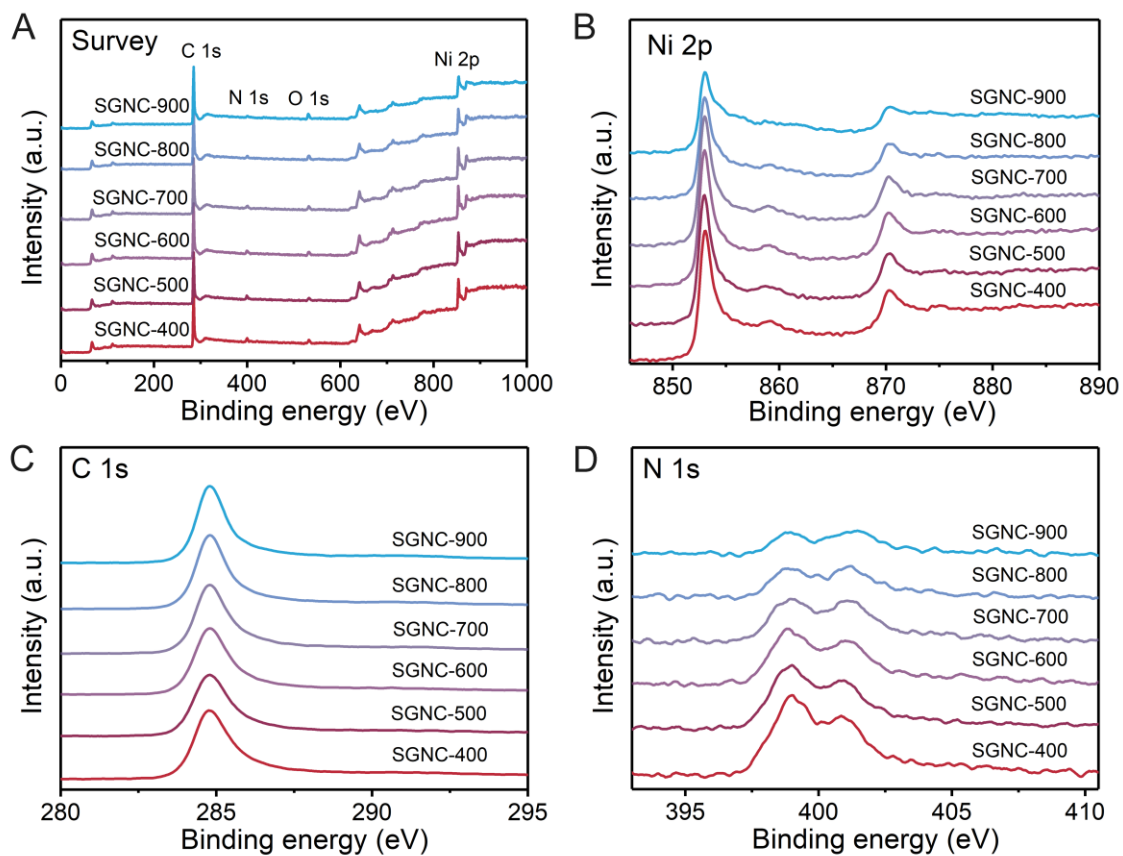


Figure S6. (A) Survey XPS spectra, (B) Ni 2p, (C) C 1s, and (D) N 1s spectra of various belt-like SGNCs.

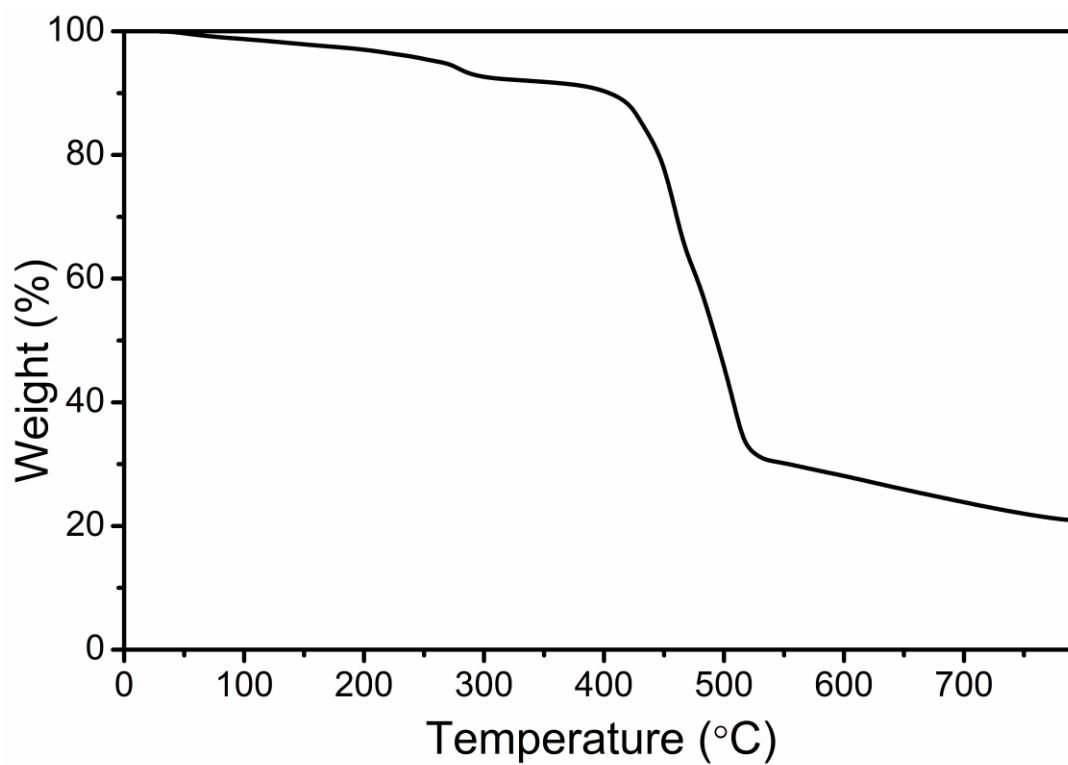


Figure S7. The TG curve pattern of the rod-shaped Ni-MOF.

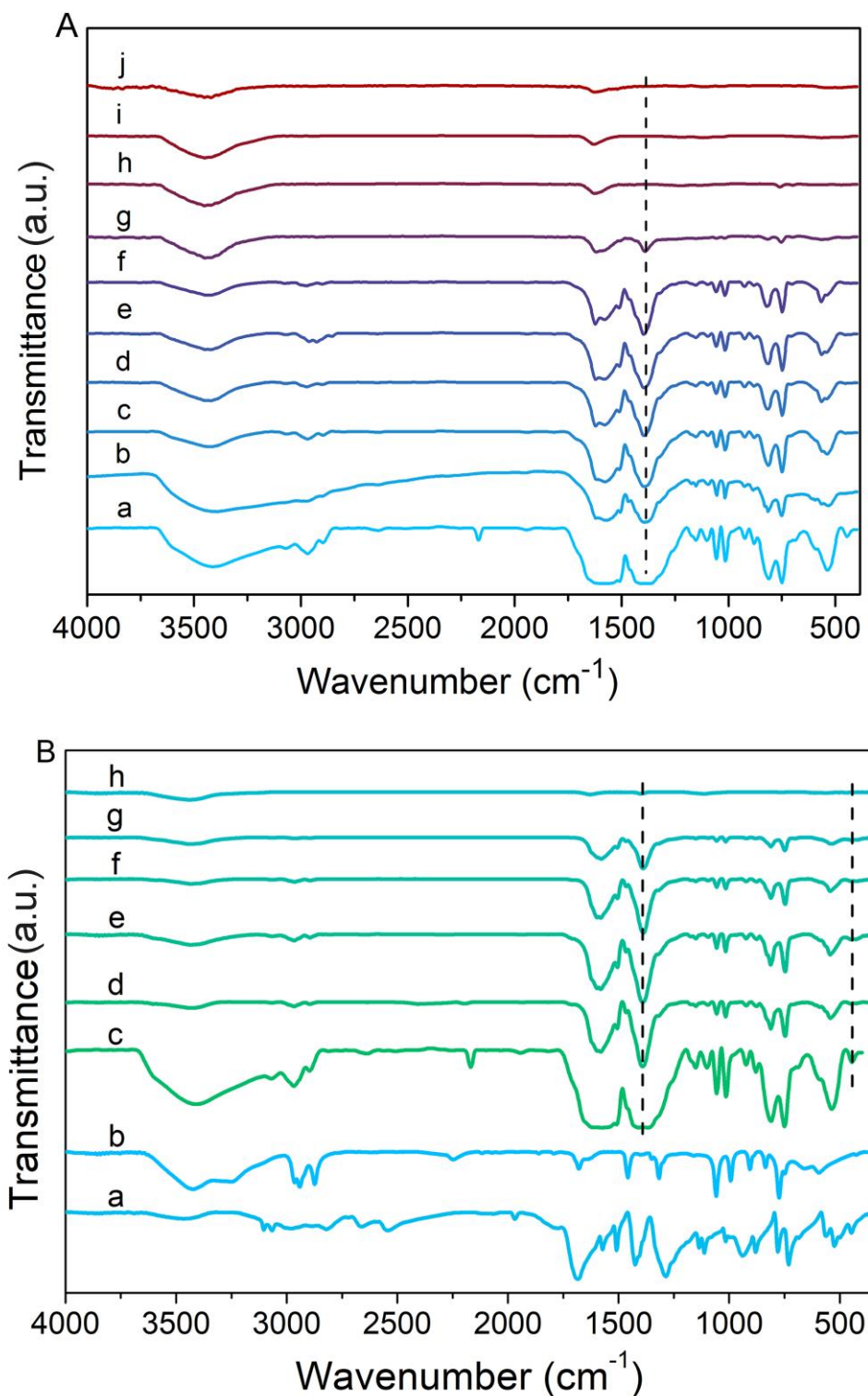


Figure S8. (A) FTIR spectra of the calcined Ni-MOF-Rod under different calcination conditions: (a) the pristine Ni-MOF-Rod, (b-g) samples carbonized at 400 °C for 5 min, 10 min, 30 min, 1 h, 2 h, and 4 h, respectively, (h) 500 °C for 4 h, (i) 700 °C for 4 h, and

(j) 900 °C for 4 h. (B) FTIR spectra of ligands and Ni-MOF-Rod calcined at different temperatures: (a) terephthalic acid, (b) Diazabicyclooctane, (c) the pristine Ni-MOF-Rod, and samples carbonized at (d) 300, (e) 325, (f) 350, (g) 375 and (h) 400 °C for 10 h.

Note: As shown in Figure S10(A), the peaks of the pristine Ni-MOF-Rod at about 440 and 1400 cm^{-1} correspond to the Ni-N bond and the $\nu_{\text{as}}(\text{C-O})$ vibrations of the $-\text{COO}^-$ groups in terephthalic acid, respectively (*React. Kinet. Mech. Catal.* **2018**, 124, 335). The peaks at around 1095 and 1057 cm^{-1} can be assigned to the C-N vibrations of dabco (*Inorg. Chem.* **2011**, 50, 5085). After calcined at 400 °C, the peak at 440 cm^{-1} in curve a disappears upon the calcination process, indicating that the Ni-N bond is broken. However, the peaks at around 1400 cm^{-1} still exist, revealing the residual carboxyl groups attached to Ni atoms. Further increasing the temperature, this band disappears attributed to the complete decomposition of organic materials.

To better understand the decomposition process of Ni-MOF-Rods, as shown in Figure S10(B), the infrared spectra of Ni-MOF-Rod calcined at a low temperature for 10 h were obtained. The results indicated that even at a low temperature of 300 °C, the peak at 440 cm^{-1} is significantly weakened, while the intensity of the peaks at around 1400 cm^{-1} is nearly no change, indicating the Ni-N bands are broken even at low calcination temperature, thus facilitating the formation of 2D layered structure which is easily exfoliated into carbon nanobelts.

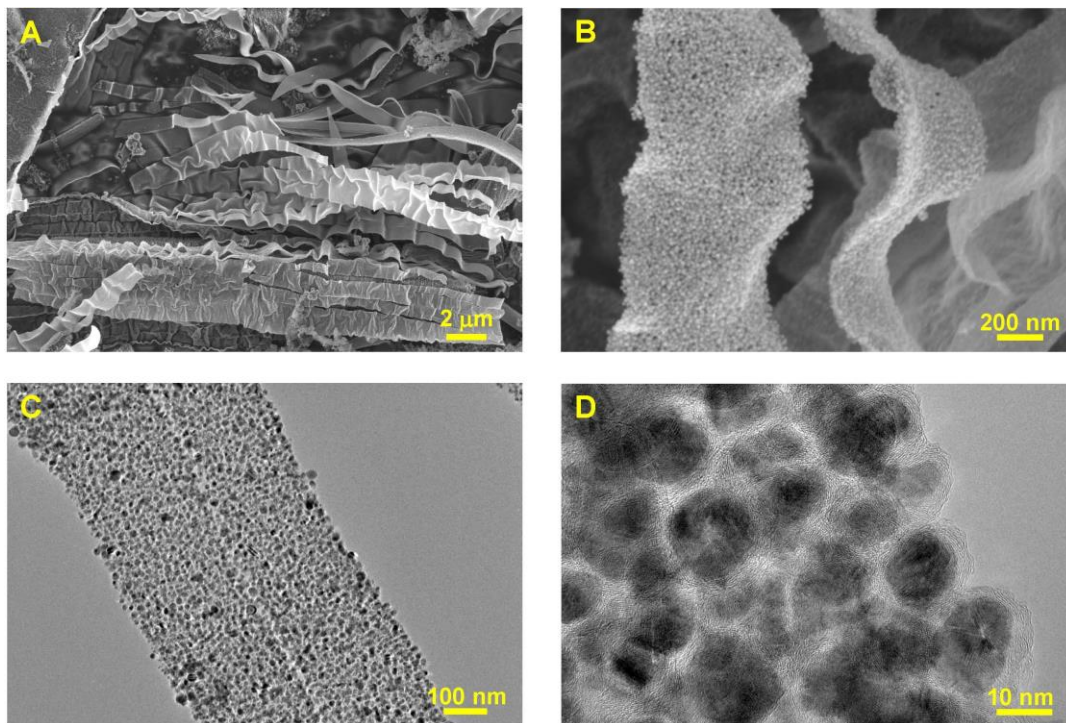


Figure S9. FESEM (A,B) and TEM (C,D) images of nanobelts obtained at 400 °C under flowing argon gas.

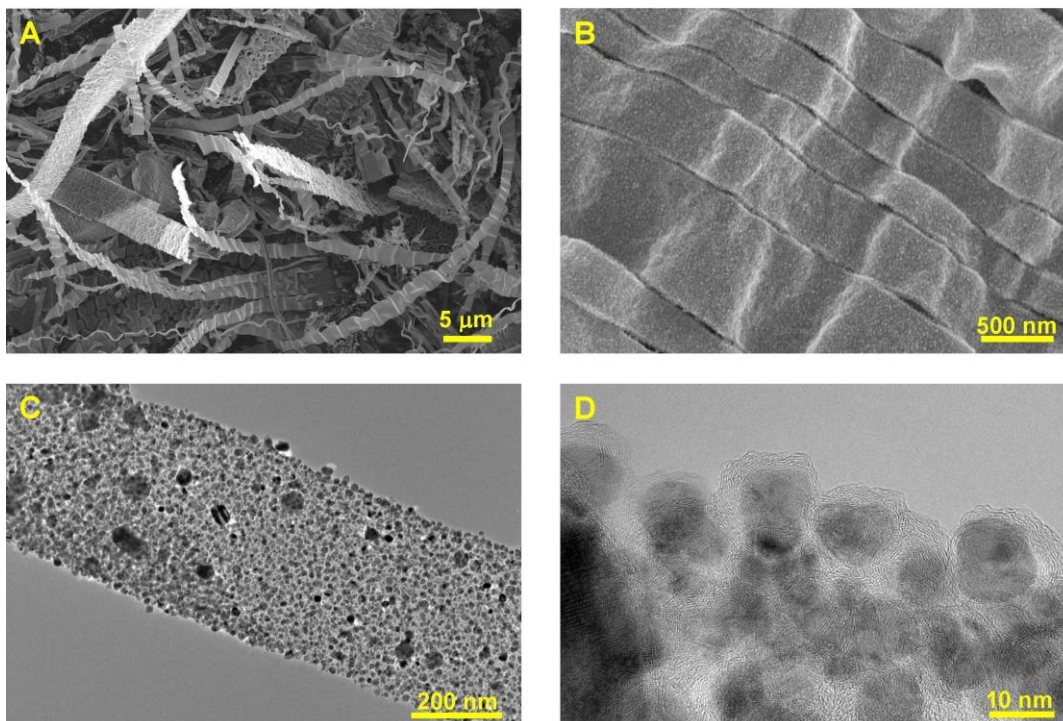


Figure S10. FESEM (A,B) and TEM (C,D) images of nanobelts obtained at 500 °C under flowing argon gas.

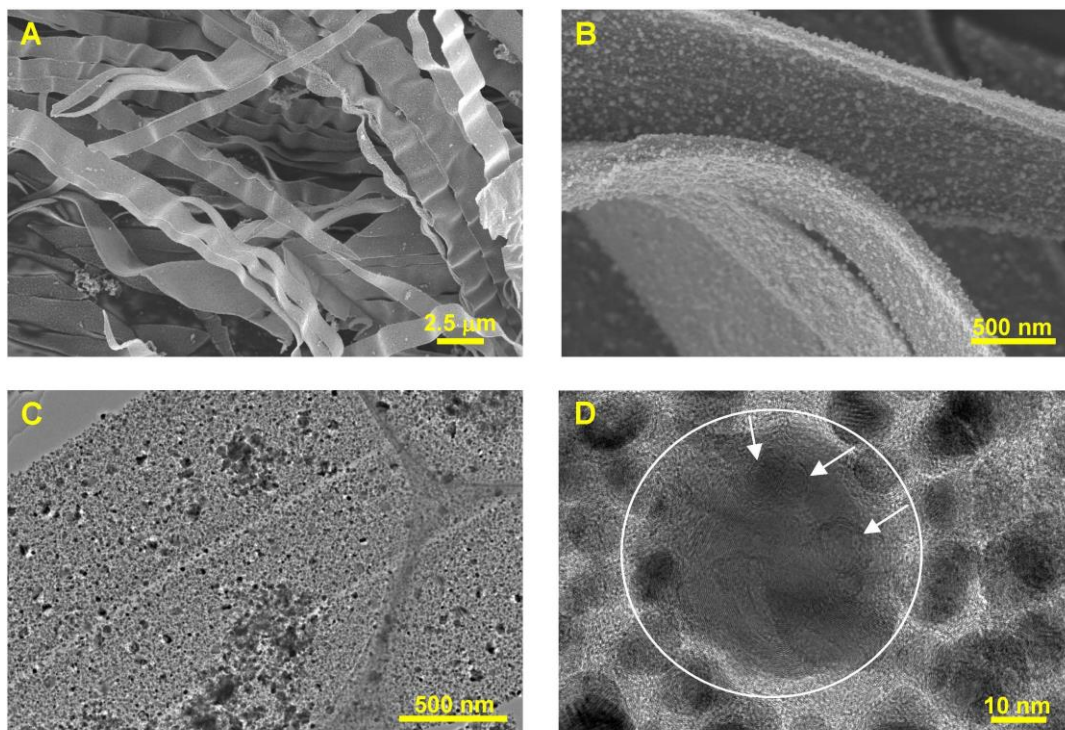


Figure S11. FESEM (A,B), TEM (C,D) images of nanobelts obtained at 600 °C under flowing argon gas.

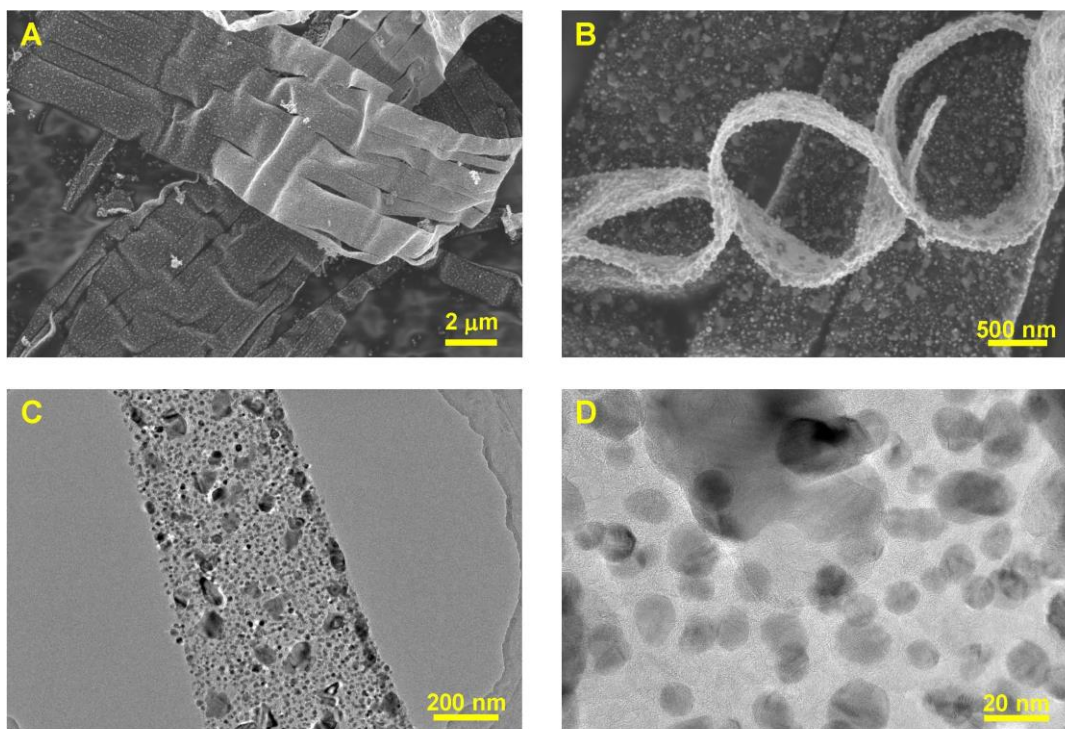


Figure S12. FESEM (A,B), TEM (C,D) images of nanobelts obtained at 700 °C under flowing argon gas.

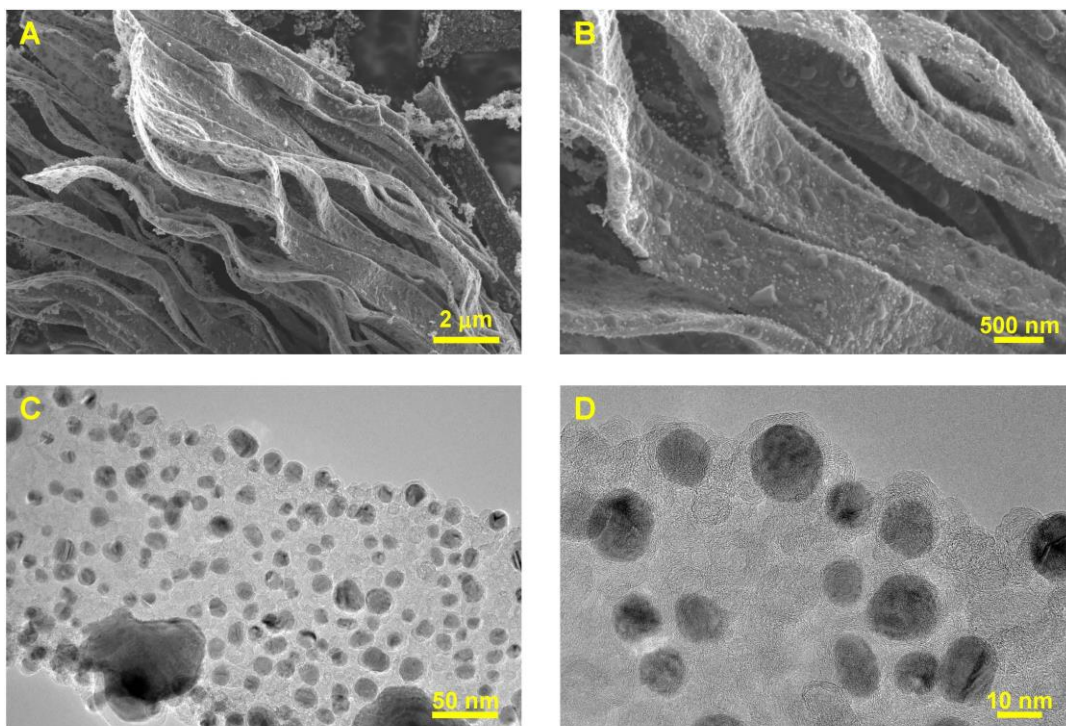


Figure S13. FESEM (A,B), TEM (C,D) images of nanobelts obtained at 800 °C under flowing argon gas.

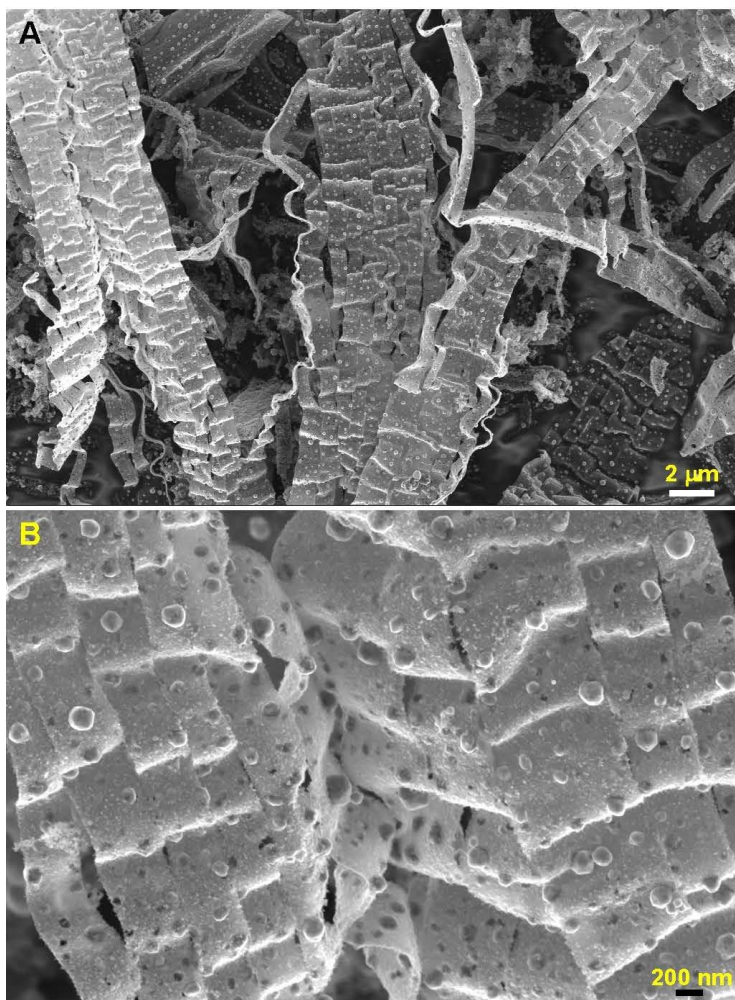


Figure S14. FESEM images of nanobelts obtained at 1000 °C under flowing argon gas.

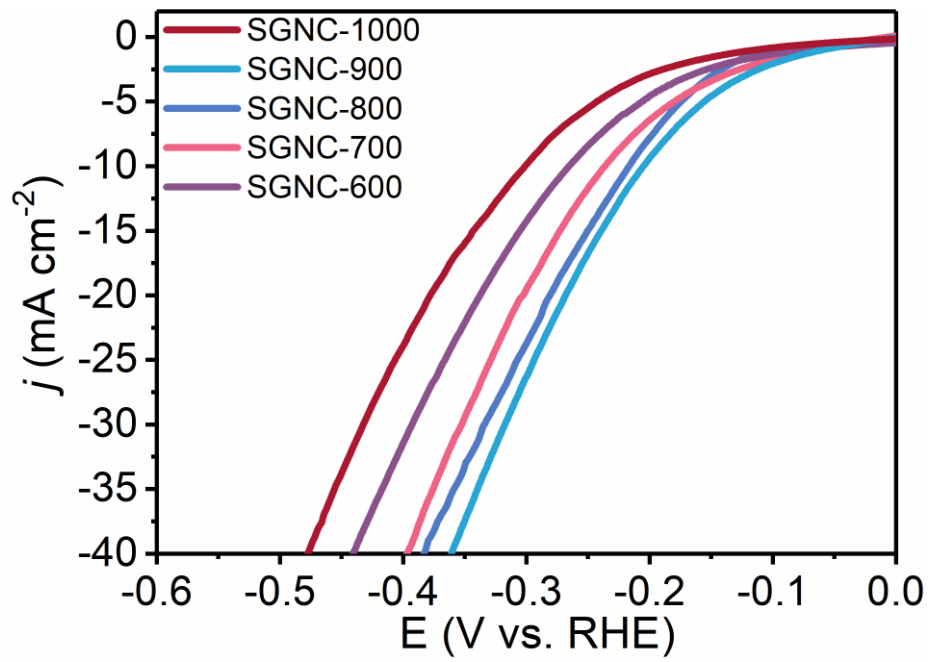


Figure S15. Polarization data of various SGNCs in 0.5 M H_2SO_4 .

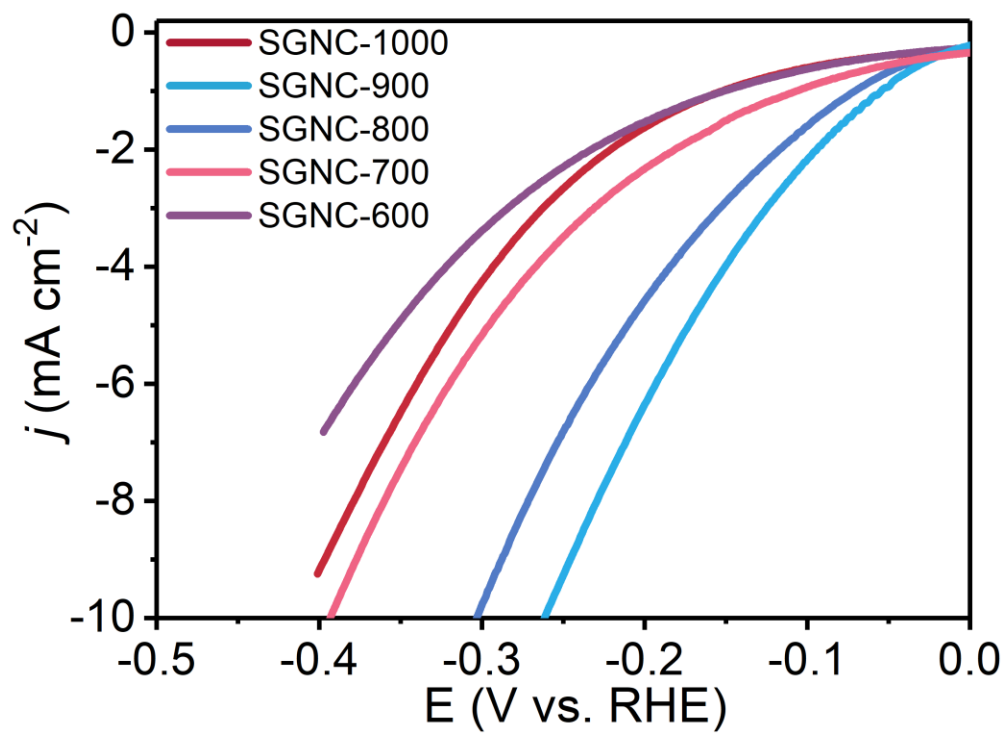


Figure S16. Polarization data of various SGNCs in 1 M PBS.

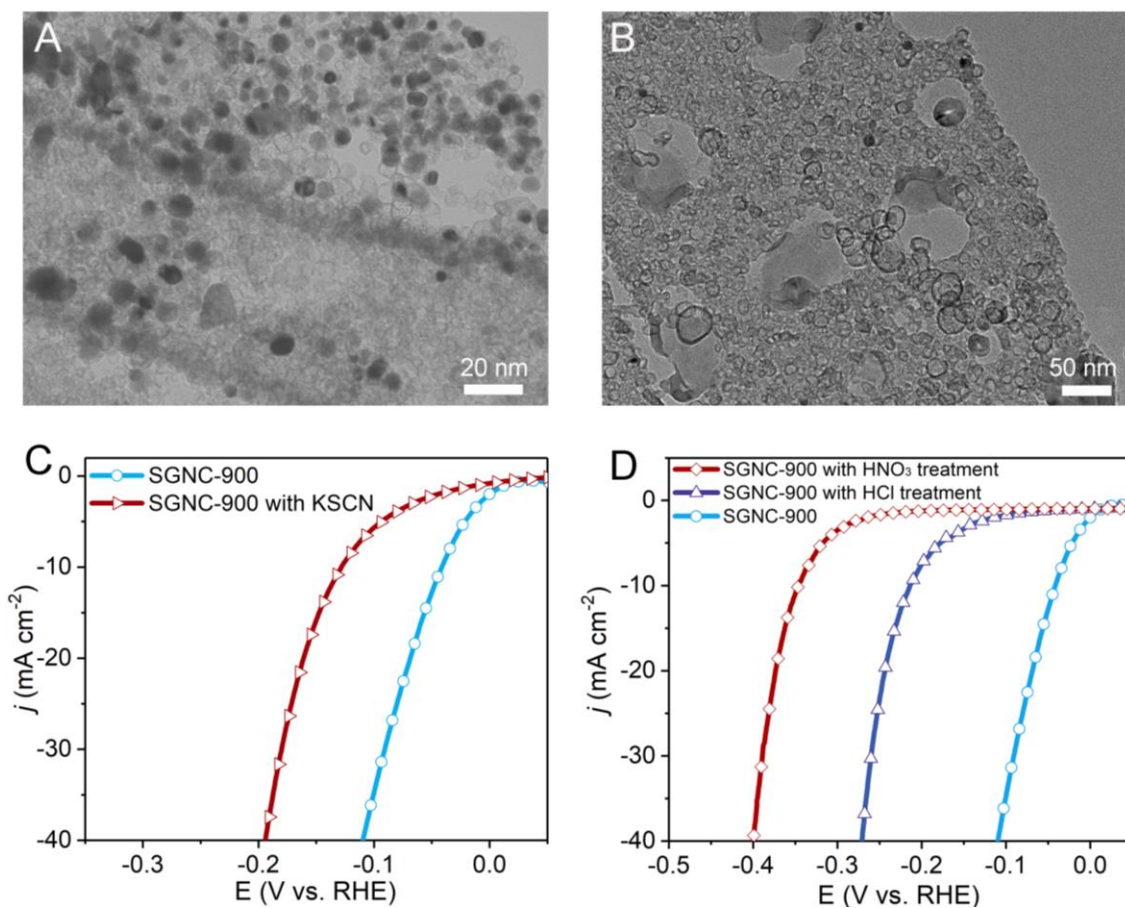


Figure S17. (A,B) TEM images of SGNC-900 treated with hydrochloric acid and nitric acid, respectively. (C) Polarization curves of SGNC-900 with and without 10 mM KSCN. (D) Polarization curves of SGNC-900 with and without acid treatment.

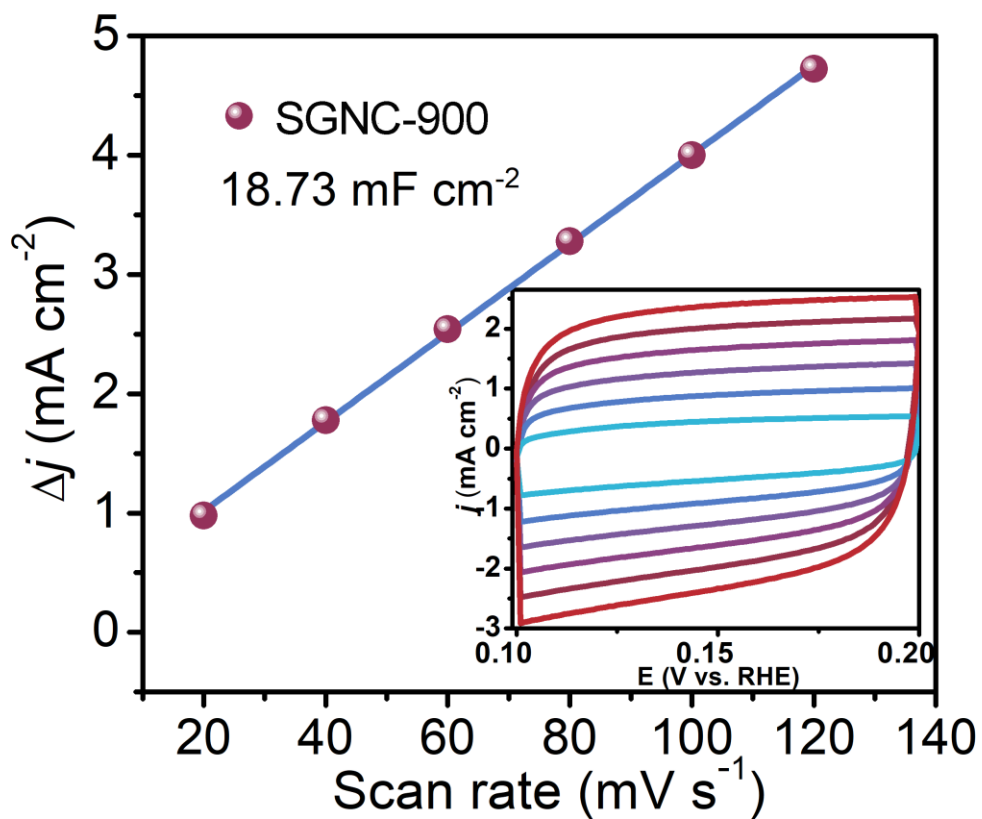


Figure S18. Plots showing the extraction of the C_{dl} for SGNC-900. The inset is CVs for SGNC-900 with different rates.

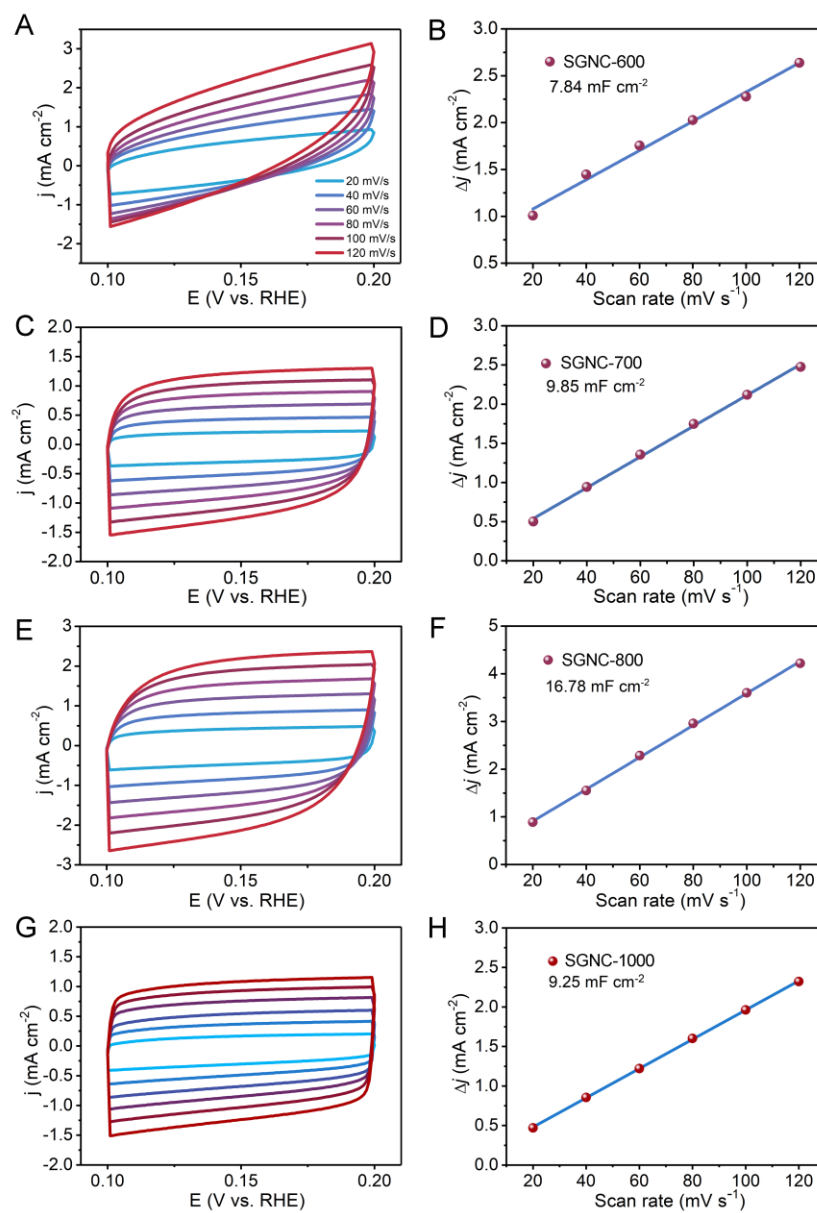


Figure S19. (A,C,E,G,I) CV conducted at potential from 0.1 to 0.2 V vs RHE. (B,D,F,H,J) The capacitive current densities measured at 0.1 V vs RHE with different scan rates. (A,B), (C,D), (E,F) and (G,H) are SGNC-600, SGNC-700, SGNC-800 and SGNC-1000, respectively.

Note: The specific capacitance obtained in Figure S19 can be converted into an electrochemical active surface area (ECSA) using the specific capacitance value for a flat standard with 1 cm² of real surface area. The specific capacitance for a flat surface

is generally found to be in the range of 20-60 $\mu\text{F cm}^{-2}$. Here we assume 40 $\mu\text{F cm}^{-2}$. The ECSA of SGNC-900, SGNC-800, SGNC-700, SGNC-600 and SGNC-1000 are 468 cm^2 , 419 cm^2 , 246 cm^2 , 196 cm^2 , and 231 cm^2 respectively.

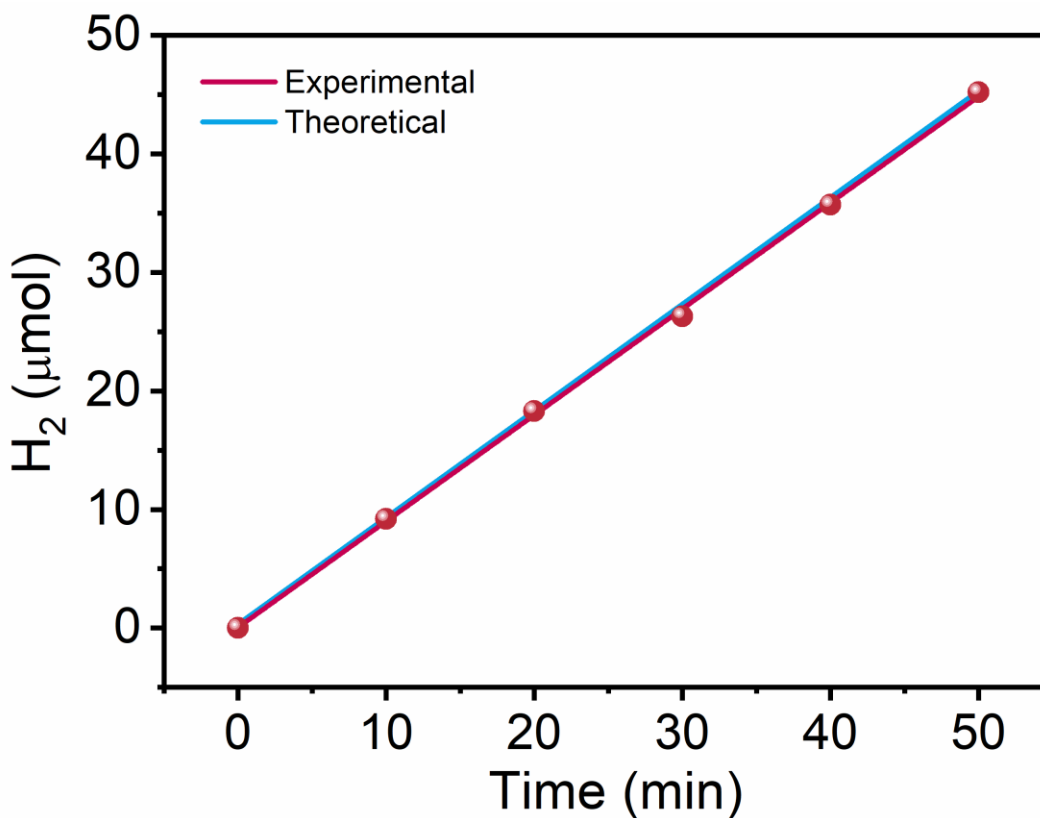


Figure S20. The theoretically calculated and experimentally measured amount of evolved hydrogen versus time for the SGNC-900.

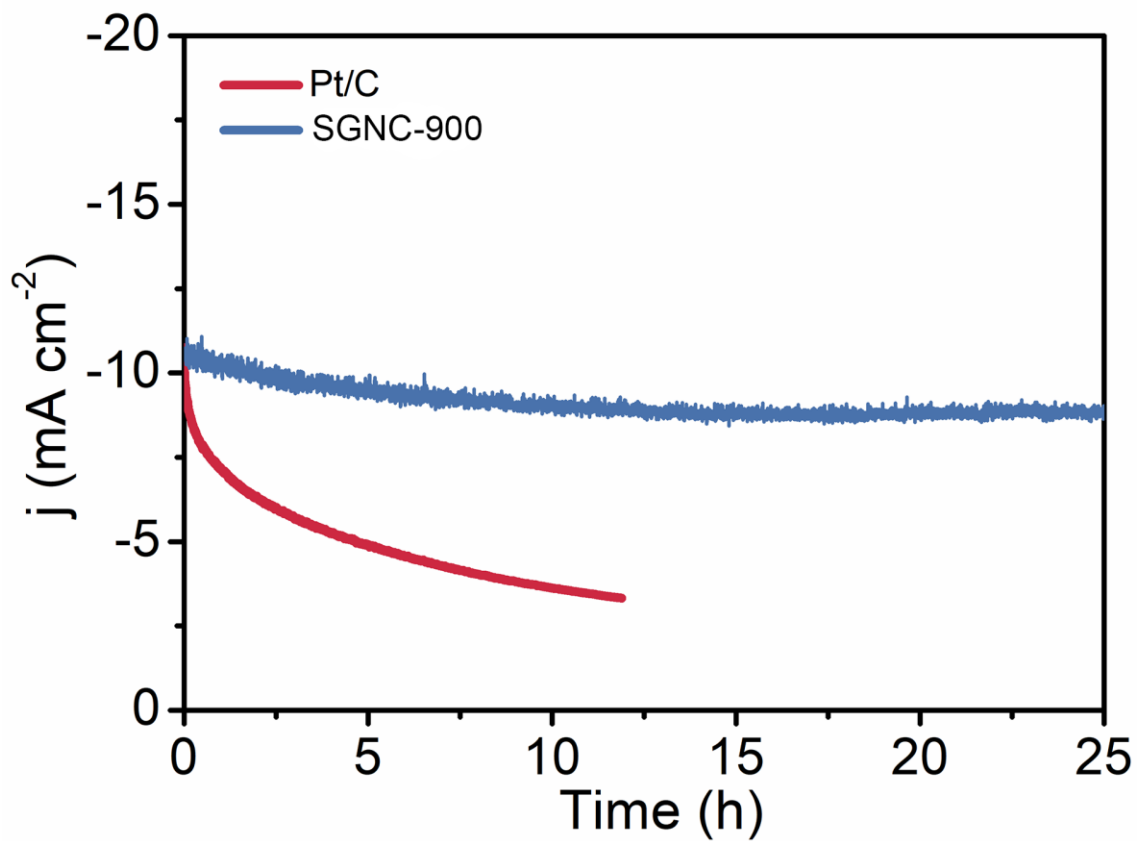


Figure S21. The time-dependent current density curves of SGNC-900 and Pt/C catalyst at the overpotential of 32 and 22 mV, respectively.

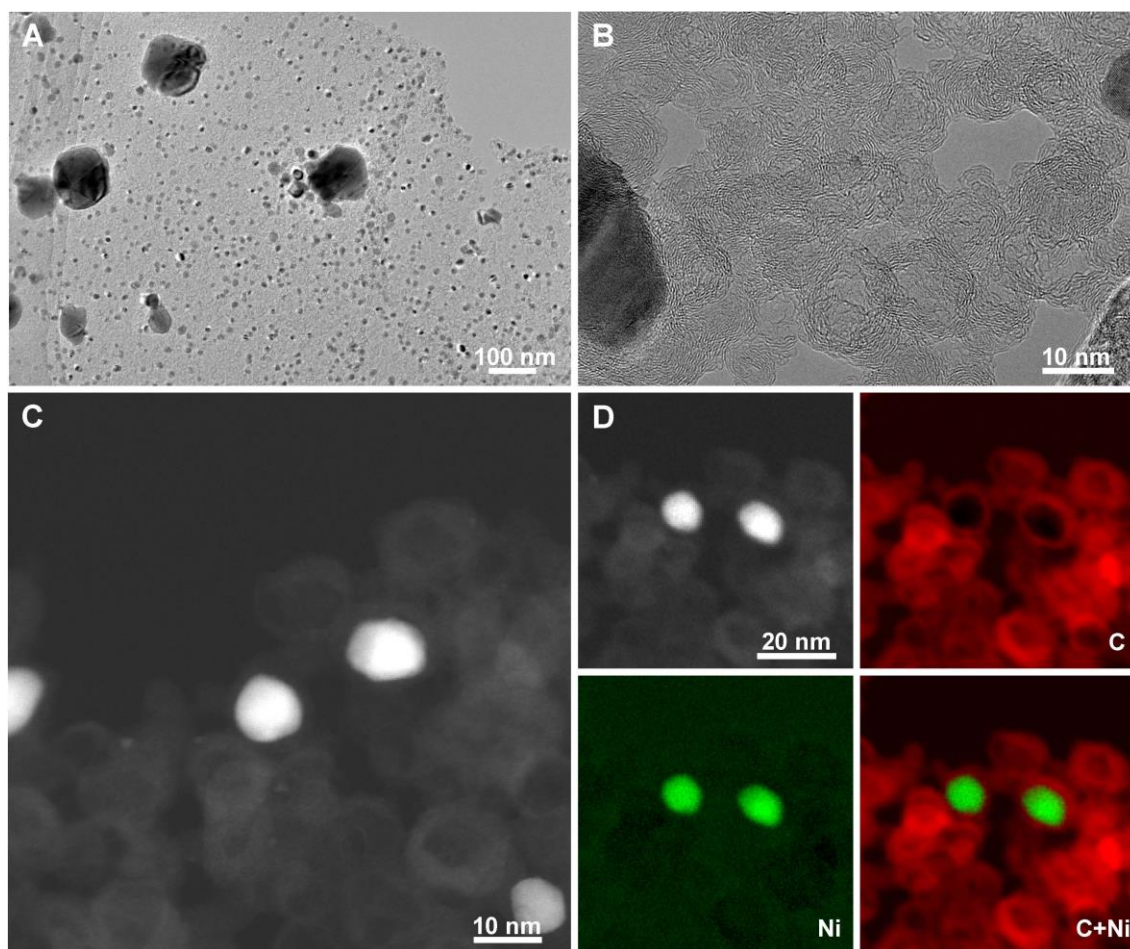


Figure S22. TEM (A), HRTEM (B), HAADF-STEM (C) of a typical carbon nanobelts and (D) the corresponding EELS maps of C (red) and Ni (green) after long-term cyclic voltammetry test.

Table S1. Elemental composition obtained from CHN analysis and high temperature oxidation method in air.^[1]

Calcination temperature (°C)	400	500	600	700	800	900	1000
C(%)	27.46	23.46	23.22	23.78	23.75	21.61	22.49
N(%)	2.22	1.67	1.45	1.14	0.80	0.47	0.28
H(%)	0.846	0.328	0.21	0.138	0.108	0.107	0.183
Ni(%)	59.0	72.3	75.3	75.1	75.5	78.0	77.2

Notes: During the high temperature oxidation treatment, the CNH is burnt out, while the Ni is converted into NiO. Based on the original mass and the obtained mass, the Ni content can be calculated.

(1) Li, J.; Li, J.; Yan, D.; Hou, S.; Xu, X.; Lu, T.; Yao, Y.; Mai, W.; Pan, L., Design of pomegranate-like clusters with NiS₂ nanoparticles anchored on nitrogen-doped porous carbon for improved sodium ion storage performance. *Journal of Materials Chemistry A* **2018**, *6*, 6595–6605.

Table S2. Comparison of catalytic parameters of AGNCs and other non-noble-metal HER composite-catalysts in alkaline media.

Catalyst	Loading (mg cm ⁻²)	Over-potential (mV)	Tafel slope (mV dec ⁻¹)	References
SGNC-900	0.6	32	39	This work
NiO NRs-m-Ov	0.2	110	100	Nano Energy. 2018, 43, 103–109.
NiOx@BCNTs	0.4	79	119	ACS Appl. Mater. Interfaces. 2017, 9, 7139–7147.
Zn _{0.30} Co _{2.70} S ₄	0.285	85	-	J. Am. Chem. Soc. 2016, 138, 1359–1365.
O-Co ₂ P	0.2	160	61	Adv. Mater. 2017, 29, 1606980.
MoS ₂ /NiCo-LDH	--	78	76	Joule 1, 2017, 383–393.
Ni(OH) ₂ /MoS ₂	0.8	80	60	Nano Energy 2017, 37, 74–80.
NiMo-EDA	0.35	72	89	ACS Appl. Mater. Interfaces. 2018, 10, 1728–1733.
NiP ₂ /NiO NRs	--	131	94	ACS Appl. Mater. Interfaces 2018, 10, 17896–17902.
Co-Ex-MoS ₂	0.2	89	53	ACS Nano 2018, 12, 4565–4573.
MoP/C	6	49	54	Adv. Energy Mater. 2018, 8, 1801258.
N-doped Ni ₃ S ₂ /NF	--	155	113	Adv. Energy Mater. 2018, 8, 1703538.
Co@N-CNTs@rGO	0.2	108	55	Adv. Mater. 2018, 30, 1802011.
R-MoS ₂	0.5	111	105	Adv. Mater. 2018, 30, 1707105.
2D-MoS ₂ /Ni(OH) ₂ -10	0.285	185	76	Adv. Mater. 2018, 30, 1801171.
holey NCP	1	58	57	J. Am. Chem. Soc. 2018, 140, 5241–5247.
o-CoSe ₂ P	1.02	104	69	Nature Comm. 2018, 9, 2533.
Co ₂ P@NPG	--	170	96	Nano Lett. 2016, 16, 4691–4698.
CoP/rGO-400	--	150	38	Chem. Sci. 2016, 7, 1690–1695.
CoP ₂ /RGO	--	88	50	J. Mater. Chem. A. 2016, 4, 4686–4690.
Nest-like NiCoP	--	68	62	ACS Catal. 2017, 7, 4131–4137.
NiCoP hollow NCs	--	150	61	Chem. Commun. 2016, 52, 1633–1636.
Ni _{0.51} Co _{0.49} P	--	82	43	Adv. Funct. Mater. 2016, 26, 7644–7651.

Ni ₂ P/Ni	--	98	72	ACS Catal. 2016, 6, 714–721.
Ni ₅ P ₄	--	49	98	Energy Environ. Sci. 2015, 8, 1027–1034.
NiSe	--	96	120	Angew. Chem. Int. Ed. 2015, 54, 9351–9355
Mo ₂ C@2D-NPC	0.738	45	46	ACS Nano 2017, 11, 3933–3942.
MoP/SNG-20	0.5	49	31	ACS Catal. 2017, 7, 3030–3038.
Cu NDs/Ni ₃ S ₂ NTs-CFs	0.52	128	76.2	J. Am. Chem. Soc. 2018, 140, 610–617.
Ni-MoS ₂ -CC	0.89	98	60	Energy Environ. Sci. 2016, 9, 2789–2793.
Mo ₂ C-C	0,84	133	82	Nano Energy 2017, 32, 511–519.
NiS ₂ hollow microspheres	0.21	219	157	J. Mater. Chem. A. 2017, 5, 20985–20992.
MoB/g-C ₃ N ₄	0.25	133	46	Angew. Chem. Int. Ed. 2018, 57, 496–500.
N-Mo ₂ C NSs	0.357	140	66	ACS Nano 2017, 11, 12509–12518.
MoP@C	0.354	81	55.6	Energy Environ. Sci. 2017, 10, 788–798.
Mo-SAs@N-Carbon	0.408	132	90	Angew. Chem. Int. Ed. 2017, 56, 16086–16090.
CoMoS	0.84	98	82	ACS Appl. Mater. Inter. 2017, 9, 5288–5294.
Co(S _{0.71} Se _{0.29}) ₂	~1	145	85.7	Adv. Funct. Mater. 2017, 27, 1701008.
Pr _{0.5} BSCF	0.232	237	45	Adv. Mater. 2016, 28, 6442–6448.
NiCo ₂ O ₄	~1	110	49.7	Angew. Chem. Int. Ed. 2016, 55, 6290–6294.
VOOH	0.8	164	104	Angew. Chem. Int. Ed. 2017, 56, 573–577.
NiP/CFP	25.8	209	129	Adv. Funct. Mater. 2016, 26, 4067–4077.
Ni ₂ P/NF	--	150	86	Angew. Chem. Int. Ed. 2016, 55, 9913–9917.
o-CoSe ₂ /CC	--	190	85	Adv. Mater. 2016, 28, 7527–7532.

